

**Benchtop venous flow model to investigate mechanical factors influencing noninvasive venous
waveform analysis (NIVA)**

By

Devin Chang

Thesis

Submitted to the Faculty of the
Graduate School of Vanderbilt University

In partial fulfillment of the requirements

For the degree of

MASTER OF SCIENCE

In

Biomedical Engineering

August 31, 2021

Nashville, Tennessee

Approved:

Bret D. Alvis, M.D.

Craig L. Duvall, Ph.D.

ACKNOWLEDGEMENTS

I would like to thank Bret Alvis for his role in mentoring and supporting my graduate academic career. Kyle Hocking is also deserving of thanks for his invaluable guidance academically and professionally. I also owe a debt of gratitude to Craig Duvall for his instrumental role in my academic successes here at Vanderbilt. I would also like to thank Joyce Cheung-Flynn for her help in harvesting and preparation of live vasculature in this project. I would like to thank Monica Polcz and Lexie Vaughn for lending me their medical expertise.

This project was funded in its entirety by Bret Alvis' NIH R01HL147244 grant.

LIST OF TABLES

Table		Page
1	Compositions of the 6% and 10% cryogels.	8

LIST OF FIGURES

Figures	Page
1. A common representation of the relationship between fluid status and morbidity risk	1
2. NIVA and PIVA waveforms captured simultaneously on a flow phantom	4
3. Cartoon of 3D printed molds used to cast the synthetic veins	5
4. Fabricated EcoFlex 00-50 vessel	6
5. Porcine Saphenous Vein was cannulated on one end with a catheter tip (A) and tied off on the other end with a suture (B).	6
6. Artificial silicone vessel cannulated on both ends with 10 Fr female urinary catheter, sealed with heat shrink tubing, and mounted within a 3D printed box.	8
7. PMF saturated in various agents for a period of 24hrs	9
8. Experimental set up for PMF model	10
9. NIVA flow waveform used in the flow loop	11
10. Plot of the variable venous flow waveform	12
11. CompuFlow 1000 interface	14
12. ΔR (mm) to pressure (mmHg) plot of the porcine saphenous vein	15
13. ΔR (mm) to pressure (mmHg) plot of the porcine saphenous vein and silicone vessels in the 0 to 50mmHg range	16
14. EcoFlex 00-30 severely distending under mild flow	16
15. %HF of PVA cryogel phantoms of 6% and 10% PVA concentration	17
16. Frequency domain analysis of PMF model	17
17. Comparison of the %HF between euvolemic and hypervolemic PMF models	18
18. Linear correlations of NIVA score and %f0 to flow rate	20
19. Effects of altering flow on NIVA score and %f0 value in a PMF model	20

LIST OF ABBREVIATIONS

%HF	Percent High Frequency
%f0	Percent composition f0
ΔR	Change in radius
DAQ	Data Acquisition (box)
DI	Deionized (water)
Ep	Peterson's Modulus
fFt	Fast Fourier Transform
FDM	Fused Deposition Modeling
GDFT	Goal Directed Fluid Therapy
GDFTdyn	Goal Directed Fluid Therapy with dynamic parameters
IV	Intravenous
IVUS	Intravenous Ultrasound
MAP	Mean Arterial Pressure
NIVA	NonInvasive Venous waveform Analysis
PCWP	Pulmonary Capillary Wedge Pressure
PIVA	Peripheral IntraVenous Volume Analysis
PMF	Porcine Myocutaneous Flap
PVA	PolyVinyl Alcohol
PVW	Peripheral Venous Waveform
SLA	Stereolithographic Apparatus
TBV	Total Blood Volume

TABLE OF CONTENTS

Acknowledgements	ii
List of Tables	iii
List of Figures	iv
List of Abbreviations	v
1 Introduction	1
2 Methods	5
2.1 Synthetic Vessel Fabrication and Validation	5
2.2 PVA Cryogel Fabrication	7
2.3 Porcine Myocutaneous Flap Preparation	8
2.4 Benchtop Flow Loop	11
2.5 Flow Waveforms	11
2.6 Statistical Tests	12
2.6.1 Synthetic Vessel Validation	12
2.6.2 PVA Cryogel: %HF	12
2.6.3 Porcine Myocutaneous Flap: %HF	13
2.6.4 Porcine Myocutaneous Flap: Flow	13
3 Results	15
3.1 Synthetic Vessel Validation	15
3.2 PVA Cryogel: %HF	16

3.3	Porcine Myocutaneous Flap: %HF Modeling	18
3.4	Porcine Myocutaneous Flap Flow Modeling	19
3.4.1	Porcine Myocutaneous Flap Flow Modeling: NIVA	19
3.4.2	Porcine Myocutaneous Flap Flow Modeling: %f0	19
4	Discussion	21
4.1	Synthetic Vein Validation	21
4.2	PVA Cryogel: %HF	22
4.3	Porcine Myocutaneous Flap %HF Modeling	23
4.4	Porcine Myocutaneous Flap Flow Modeling	25
5	Future Work	27
6	Conclusion	28
7	References	29

1) Introduction:

Administration of intravenous fluid intraoperatively is necessary to maintain intravascular volume in the face of losses due to factors such as fasting, urine output, and hemorrhage. Hypovolemia leads to poor organ and peripheral tissue perfusion resulting in organ dysfunction and shock.¹ However, liberal fluid administration can lead to hypervolemic states, putting patients at increased morbidity and risk of complications.² Generally speaking as plasma volume increases, water and electrolytes migrate out of intravascular space and into the interstitial space. The rising plasma volume is kept in check by renal excretion, which in turn draws fluids back

out from the interstitial space into the intravascular compartment. Many factors can affect this balance, including anesthetic and analgesic drugs, dehydration, hemorrhage, gender, and type of fluid infused.^{3,4} For example, unconscious patients may have a hourly urinary excretion rate of 50-100mL after 1 to 2L of infused fluid while conscious patients may have a hourly urinary excretion rate of ten times that.⁴ When it comes to the choice of infused fluid, the

time to first void for saline is two times longer than Ringer's lactate and three times longer for 5% glucose.^{3,5,6}

A common representation of the complications associated with volume status is a U-shaped curve on which the x-axis represents increasing volume load and the y-axis represents morbidity risk. **(Figure 1)** Optimization of fluid balance can be represented by a horizontal line that separates the upper "arms" of the curve from the curve valley. The curve below the line represents an ideal volume range for an individual patient in order to maintain optimal postoperative outcomes.⁷

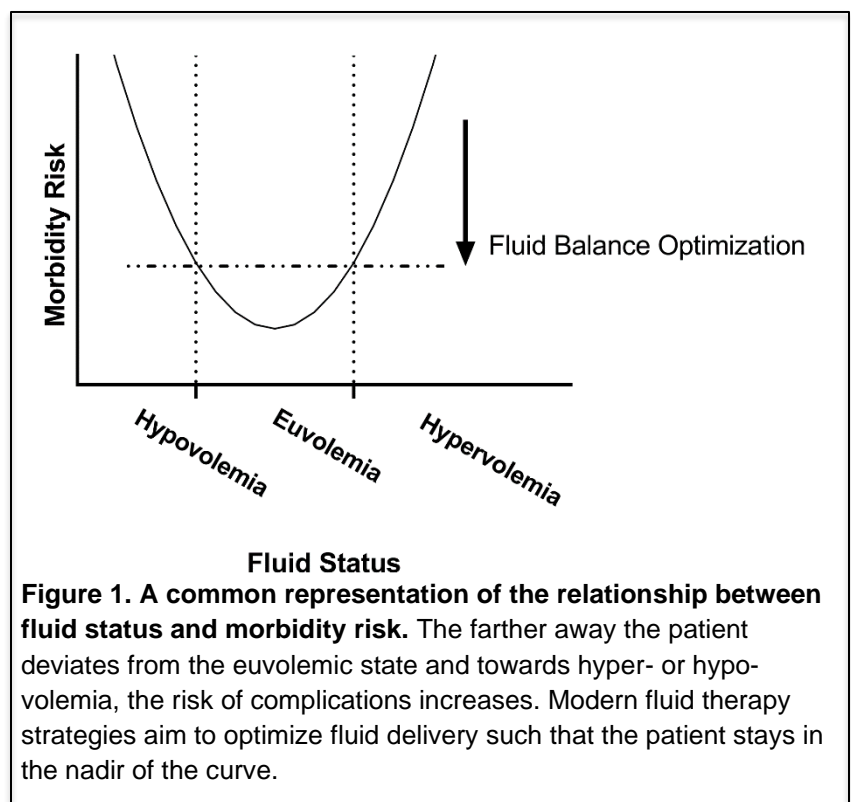


Figure 1. A common representation of the relationship between fluid status and morbidity risk. The farther away the patient deviates from the euvoemic state and towards hyper- or hypovolemia, the risk of complications increases. Modern fluid therapy strategies aim to optimize fluid delivery such that the patient stays in the nadir of the curve.

Conventional fluid therapy is guided on parameters that include mean arterial pressure (MAP), heart rate, and diuresis. These parameters have been found to be lacking; detection of hypovolemia only occurs after a loss of 20% total blood volume (TBV), while blood pressure and heart rate do not react to fluid overload in patients without heart failure.¹

Goal-directed fluid therapy (GDFT) is an effective method in optimizing fluid balance and has been shown to reduce morbidity risk as compared to conventional fluid therapy.^{8,9} A meta-analysis on goal-directed fluid therapy with dynamic parameters (GDFTdyn) found a reduction in post-operative morbidity (OR 0.51, CI 0.34 to 0.75; $p < 0.001$, $n = 961$) stemming from a reduction in infections, cardiovascular, and abdominal complications. The analysis also found a decrease in length of ICU stay (WMD -0.75 days; CI -1.37 to -0.12, $p = 0.02$).⁸

GDFT operates on cardiovascular measurements such as stroke volume, arterial waveform analysis, and stroke volume variation.^{1,10,11} Unfortunately, these outmoded methods fall short in a number of ways. Clinical signs such as jugular venous distension, dyspnea, and elevated central venous pressure lack specificity and sensitivity to volume overload.^{12,13} Furthermore, techniques such as arterial pulse-pressure variation waveform analysis are accurate only in mechanically ventilated patients with high tidal volume.¹⁴ Another volume assessment metric, pulmonary capillary wedge pressure (PCWP), is obtained via a balloon inserted via central venous catheter and inflated in the right atrium. PCWP remains the clinical gold standard for intravascular volume assessment, but is a highly invasive procedure and is susceptible to subjective interpretation of the pressure tracings.^{15,16,17,18} As a result, there remains an unmet need for a reliable, minimally invasive method for volume assessment to guide GDFT.

Peripheral venous waveform (PVW) analysis has emerged as a novel solution to this clinical need.^{19,20,21,22,23,24,25,26} The venous system as a whole is responsible for containing ~ 60-70% of total blood volume (TBV), with the reactive venous reservoir containing ~ 45% TBV.²⁷ The vasculature in this reservoir exhibits high mechanical compliance (110mL/mmHg vs 4mL/mmHg in the central venous compartment)²⁸ which in combination with venous tone control allows the body to maintain stroke volume. Considering the

significant role, the venous compartment plays in storing TBV, it stands to reason a deeper analysis of the venous compartments may yield a relationship to TBV.

Two methods of PVW capture are known as peripheral IV analysis (PIVA) and non-invasive venous waveform analysis (NIVA). PIVA relies on an indwelling venous catheter whereas NIVA relies on a noninvasive piezo-crystal sensor placed on the volar aspect of the wrist.²³ NIVA has been demonstrated to be able to accurately detect 500mL of loss in adult blood donors (92% sensitivity, 84% specificity, n =50)²⁴ while PIVA correlates with volume removed during hemodialysis ($R^2=0.77$, n =37).¹⁹ In both methods, the captured PVW is transformed to the frequency domain to analyze the relative contributions of each frequency to the overall waveform. The PVW in the frequency domain exhibits a fundamental pulse frequency (f_0) and associated harmonic frequencies (f_1 - f_7), which together are thought to be representations of physiological cardiac events given some morphological similarities to the central venous pressure waveform.²⁶

NIVA scores are currently generated from the lower harmonics.^{23,24,25} In the blood donor study, NIVA score was computed on the relative contributions of f_0 - f_2 as follows:

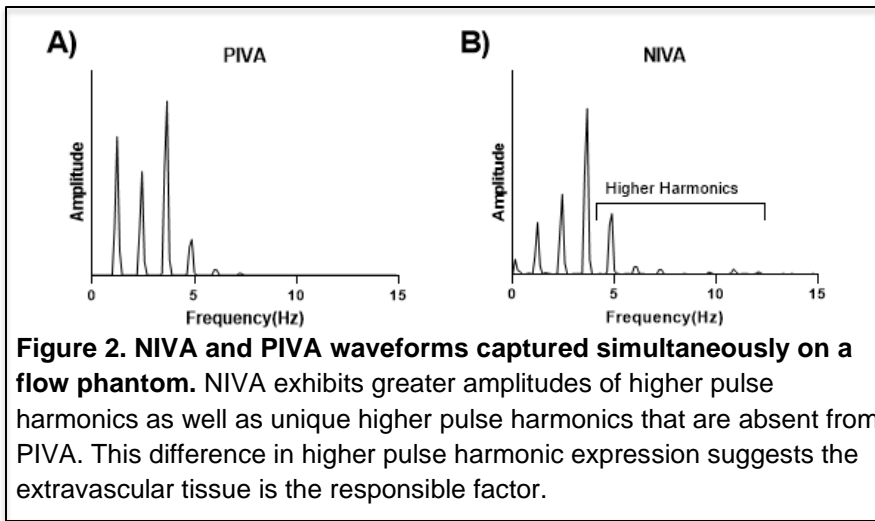
$$\text{NIVA} = (2*f_0+0.4*f_1+0.2*f_2)/\text{sum}(f_0:f_2) \quad (1)$$

A key finding in that study was that NIVA scores decreased following 500mL of blood donation ($p < 0.05$, n = 50).²³ It was noted that the power of the fundamental pulse frequency, f_0 , decreased relative to the f_1 and f_2 harmonics leading to the drop in NIVA score. The contribution of f_0 to the overall NIVA signal ($\%f_0$) can be quantified as:

$$\%f_0 = f_0/\text{sum}(f_0:f_2)*100 \quad (2)$$

Studies have shown that in the face of acute hemorrhage, the pressure gradient between mean circulatory pressure and central venous pressure decreases.^{29,30} This pressure gradient is responsible for driving venous return, so decreases in the gradient should result in decreases in venous flow.^{29,30,31} It is hypothesized that

decreasing flow in a benchtop venous flow model would result in decreased NIVA scores and a decrease in %f0.



A unique feature of NIVA waveforms as opposed to PIVA waveforms is the presence of higher pulse harmonics (f3-f7) in the NIVA signal observed in volume overloaded patients. **(Figure 2)** Considering the difference in waveform transduction between NIVA and PIVA, it is likely that

the presence of the higher pulse harmonics is due to the resonance of the extracellular matrix. The relative power of the higher pulse harmonics (%HF) is calculated as:

$$\%HF = \frac{\text{sum}(f3:f7)}{\text{sum}(f0:f7)} * 100 \quad (3)$$

It is hypothesized that an edematous state would result in increased %HF as compared to an euvoletic state.

2) Methods:

A phantom that would allow for a benchtop simulation of peripheral venous flow was created to investigate the influence volume status has on the NIVA waveform. This *ex vivo* model consisted of synthetic vessels representing the veins, a substrate for the vein to be embedded within to represent the extracellular matrix, and a pump to generate physiologically accurate flow through the phantom.

2.1) Synthetic Vessel Fabrication and Validation

Given the relative difficulty in obtaining fresh vasculature, synthetic vessels were cast in 3D-printed molds from a variety of silicones (Smooth-On, Macungie, USA) including EcoFlex 00-30, EcoFlex 00-50, and

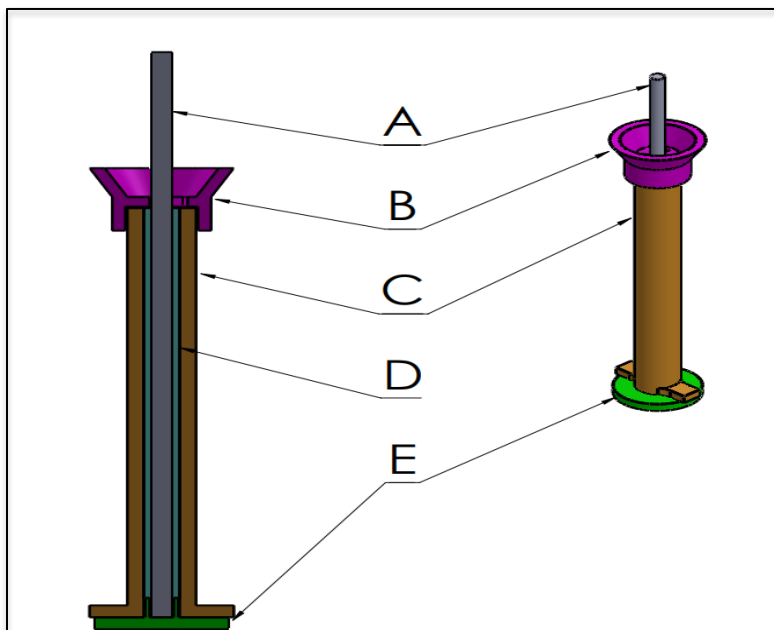


Figure 3. Cartoon of 3D printed molds used to cast the synthetic veins (left: section view, right: isometric view) printed on a combination of SLA (Formlabs Form 2, Tough Resin, Somerville, MA, USA) and FDM (Ultimaker 3, PLA, Utrecht, Netherlands) machines. The molds consisted of a A) steel rod core, B) SLA vent cap, C) FDM body, and E) SLA bottom cap; all of which were treated with a mold-release agent. This design resulted in a D) silicone vessel with the following dimensions: 5.475mm OD, 3.175mm ID, ~75mm overall length.

OOMOO-25. The EcoFlex 00-30 and 00-50 have durometer ratings on the Shore 00 hardness scale of 00-30 and 00-50 respectively. The OOMOO-25 silicone is graded on the stiffer Shore A hardness scale at 25A. All silicone was degassed prior to pouring into the mold and was pressurized to 30 PSI while in mold for a period of 24 hours. All of the mold components including the steel rod core were treated with Stoner E436 (Stoner International, Chai Wan, Hong Kong) to facilitate easier part release. **(Figure 3)** This process resulted in vessels with the following dimensions: 5.475mm outer diameter, 3.175mm inner diameter, and approximately 75 mm in

overall length. The EcoFlex 00-30 and 00-50 silicones are translucent and can be visually inspected for voids. If the steel core rod was misaligned and not uniformly concentric to the mold body, the resultant vessel would have a varying diameter that can be detected at either end of the vessel by rolling each end between one's fingertips and the vessel can subsequently be removed from further testing. **(Figure 4)**

The silicone vessels were verified to be valid approximations of real tissue using methods described in

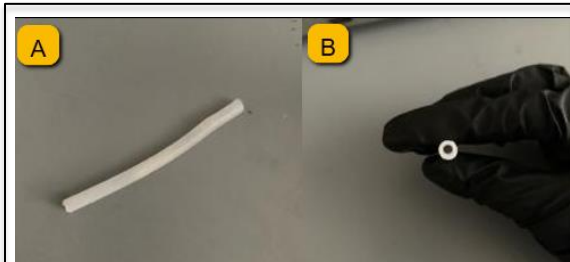


Figure 4. Fabricated EcoFlex 00-50 vessel. (A) The EcoFlex series of silicones are translucent, allowing for visual inspection for internal voids. (B) A simple check for vessel wall uniformity is done by rolling each end of the vessel between ones fingertips.

literature.^{32,33} Porcine saphenous veins freshly harvested under an approved Institutional Animal Care and Use Committee protocol (IACUC # M1800176-00) and transported in Plasmalyte solution (Baxter International Inc., Deerfield, IL, USA) were cut to a relaxed length of 50mm and were cannulated on one end with a catheter tip secured with suture (5-0, Ethicon, Raritan, NJ).

The catheter tip was attached to a three way stopcock connected to a pressure sensor and a 5mL syringe containing

deionized (DI) water. **(Figure 5)** DI water was flowed through the catheter to displace all air within the vein and catheter tip before the open end of the vein was tied off with suture. The entire system was secured with surgical tape to a laminated backdrop that had a high-contrast pattern printed on it. In this position, the veins were stretched to 60mm, which corresponds to a 20% increase in length that is consistent with in-vivo conditions.³⁴

While the vein was manually pressurized with the syringe, the intraluminal pressure was recorded by the catheter pressure sensor connected to a PowerLab Data Acquisition box (ADInstruments, Sydney, Australia) sampled at 1 kHz and the change in radius was recorded by a camera

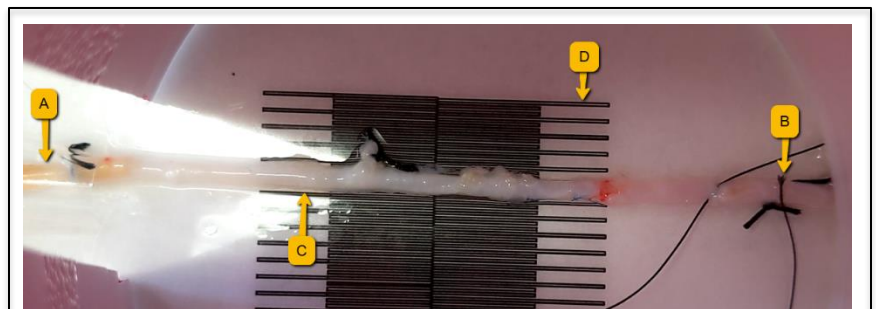


Figure 5. Porcine Saphenous Vein was cannulated on one end with a catheter tip (A) and tied off on the other end with a suture (B). The vein (C) was stretched to 120% of the relaxed length before the vessel was pressurized with DI water. Longer tick marks (D) on the background are 0.4mm wide and spaced 2.4mm apart, allowing the change in radius with the increasing pressure to be calculated.

mounted directly overhead the patterned area of the backdrop. Pressures were recorded at intervals of 5 mmHg from 0 to 50 mmHg and subsequently at intervals of 10 mmHg from 50 to 100 mmHg. This process was essentially repeated with all the synthetic silicone vessels, the only difference being the usage of a modified catheter tip and a 3D-printed end plug to ensure the proper sealing of the synthetic vessel.

The Peterson's modulus (E_p) relates the intraluminal pressure (stress) and vessel diameter expansion (strain) as follows:

$$E_p = \Delta P / (\Delta D / D_0) \quad (4)$$

where ΔP is the change in pressure and $\Delta D / D_0$ is representative of the change in diameter respective to the original diameter.^{35,36} The Peterson's modulus defines elastic behavior by normalizing the physical dimensions of the test object. However, in some benchtop modelling such as venous flow or vessel stiffness studies it is valuable to have vessels that can accurately mimic the absolute deflection veins can achieve. Calculation of change of radius (ΔR) to pressure slopes allows for quantification of both the absolute rate and absolute deflection of a vessel.

2.2) PVA Cryogel Fabrication

Prior work utilized an agar gel to model the extracellular matrix. The agar was mixed in two different concentrations (1% and 3%) to simulate a normal state and edematous state respectively. With a human saphenous vein imbedded within the agar gel and the entire model connected to a roller pump, greater contribution of higher frequencies was observed in the 3% as compared to the 1% agar gel in NIVA recordings (52.48% vs 25.71%, $p < 0.05$, $n=5$), and no substantial difference in higher frequency contribution was observed between either gel in PIVA recordings.

However, one issue with this model is the rather large difference in material stiffness between the 1% and 3% agar gels. The 1% gel had a Young's modulus of 175.0 mmHg while the 3% had a modulus of 5250.5 mmHg. PVA cryogel, a mix of polyvinyl alcohol, ethanol, and deionized water, has been shown to exhibit elastic modulus properties similar to those of biological fatty and glandular breast tissues.³⁷ Additionally, these

cryogels can be more finely tuned to alter their stiffness by varying the concentration of PVA in the gels. The cryogel exhibits a Young's modulus ranging from 97.5 mmHg at 6% PVA concentration to 397.5 mmHg at 10% PVA concentration while at 15% strain, which mirror fatty and glandular breast tissue respectively.³⁷

In the PVA cryogel phantom, the silicone vessel was mounted in a 3D printed enclosure via cannulation at both ends by modified 10 Fr female urinary catheters (Cure Medical, Newport Beach, CA). Each end was tied off with suture then sealed over with heat shrink tubing.

(Figure 6) The PVA cryogels were synthesized starting with a DI water to ethanol ratio of 50:50 by weight normalized to 100 g total mass for the desired concentration. **(Table 1)** The mixture was covered and continuously stirred for 2h at 90 C until homogenous before being poured to the brim of the 3D printed enclosure. The assembly was then subjected to four freeze thaw cycles consisting of 12 hrs at -20 C followed by a thaw at room temperature (23 C) for 4hrs.



Figure 6. Artificial silicone vessel cannulated on both ends with 10 Fr female urinary catheter, sealed with heat shrink tubing, and mounted within a 3D printed box. The enclosure was then filled with PVA cryogel solution and subjected to four freeze-thaw cycles to form the gel. The top two phantoms pictured are 10% PVA cryogels, while the bottom two phantoms shown are 6% PVA cryogels.

<i>Cryogel</i>	<i>PVA (g)</i>	<i>EtOH (mL)</i>	<i>DI-H₂O</i>
6%	6	60.83	48
10%	10	57	45

Table 1: Compositions of the 6% and 10% cryogels.

2.3) Porcine Myocutaneous Flap Preparation

The PVA cryogel was not the only model used to simulate the extracellular matrix. Porcine Myocutaneous Flaps (PMF), colloquially known as pork belly, was investigated as a possible alternative

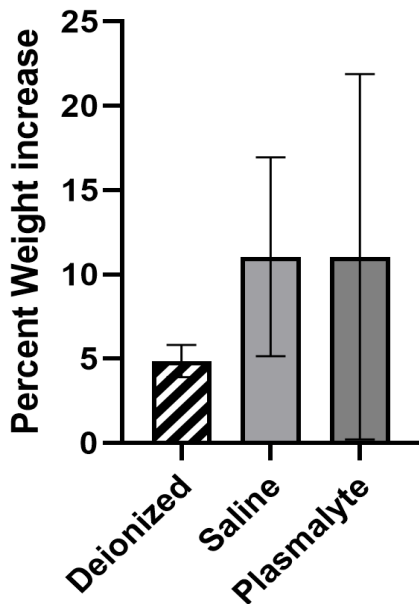


Figure 7. PMF saturated in various agents for a period of 24hrs. Saline and Plasmalyte both caused the highest uptake of fluid of 11%±1.37 (n = 3) and 11%±2.52 (n = 3) respectively. However, the saline demonstrated a more consistent fluid uptake with a smaller standard deviation (1.37 vs 2.52). An unpaired two-tailed t-test demonstrated the fluid uptake in saline was significantly greater than in DI. ($p < 0.05$, $n = 6$)

substrate to embed the veins in. PMF (K&S World Market, Nashville, TN) was sectioned into chunks (~40mmx60mmx35mm) and cut such that the muscle fibers ran parallel to the major axis of the section to maintain consistency. These PMF sections were bathed in various agents for a period of 24hrs at 4C to determine which would cause the greatest uptake of fluid to mimic an edematous state. 0.9% saline was found to consistently increase mass of PMF the most at 11%±1.37 (n=3). **(Figure 7)** The artificial vessel was tunneled into PMF for preliminary testing with hemostatic clamps. With the vessel in place, the PMF was mounted into another 3D printed enclosure and cannulated with the same modified 10Fr female urinary catheters.

2.4) Benchtop Flow Loop

In both PVA cryogel and PMF models, the piezo-crystal sensor was taped to the phantom and a pressure sensor was placed in-line with the flow loop to measure intraluminal pressure. Both sensors

streamed and recorded data to a laptop via an PowerLab Data Acquisition Box (ADInstruments, Sydney, Australia) at a sampling rate of 1kHz. **(Figure 8)** The captured flow signal was transformed from the time domain into the frequency domain using LabChart 7 software (ADInstruments, Colorado Springs, CO) by fast Fourier Transform with 8k windows. A positive displacement flow pump (Compuflow 1000, Shelley Medical Imaging Technologies, London, Canada) equipped with an internal reservoir vented to atmospheric pressure was used to generate flow.

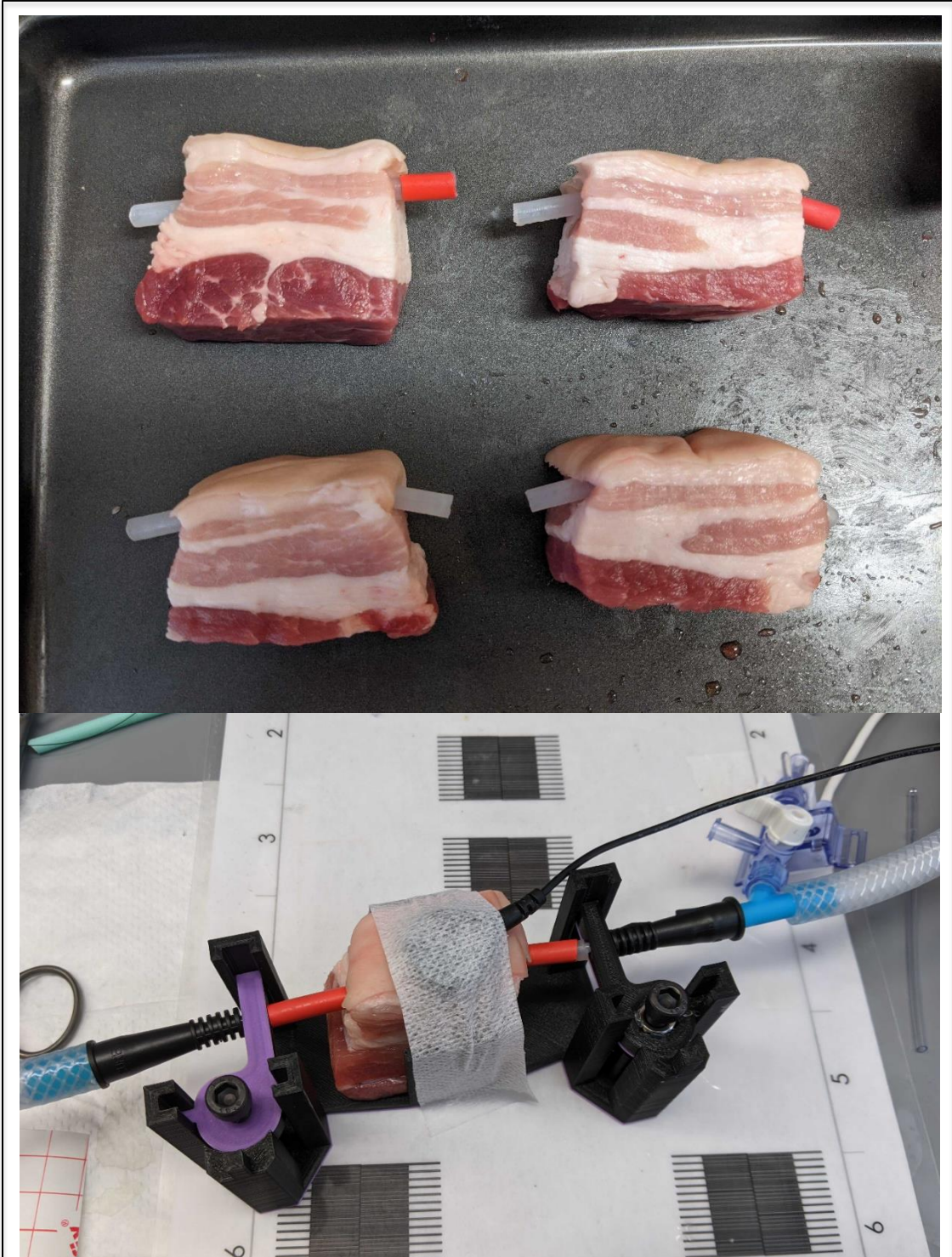
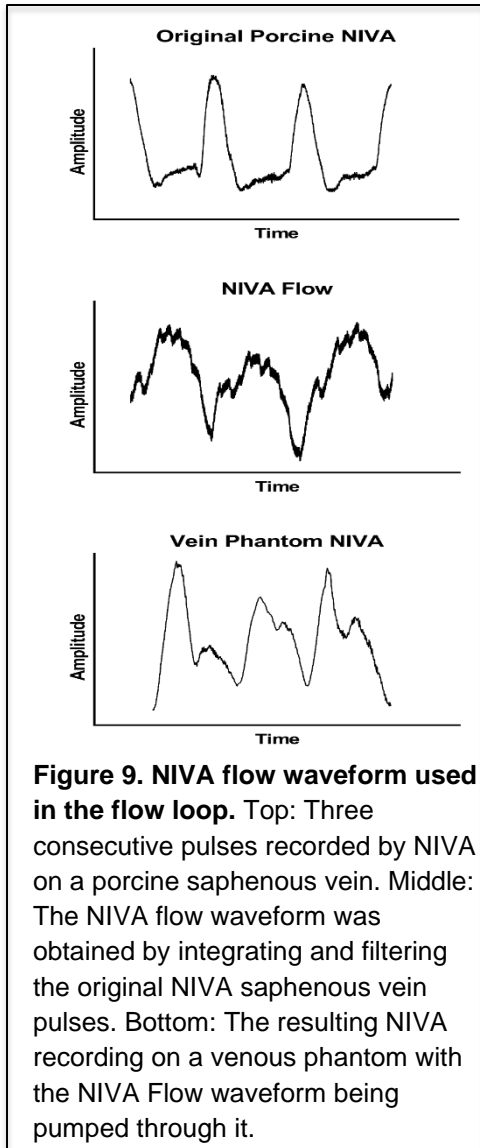


Figure 8. Experimental set up for PMF model. Top: Several PMF cuts with silicone veins tunneled into them. Bottom: A PMF containing a tunneled silicone vein is connected into the flow loop and connected to a piezo-crystal sensor and an in-line pressure sensor to capture NIVA and PIVA signals respectively. Set screws on either end of the flow loop allowed for the inlet and outlet ports to be height adjusted to suit the variations across the flaps.

2.5) Flow Waveforms

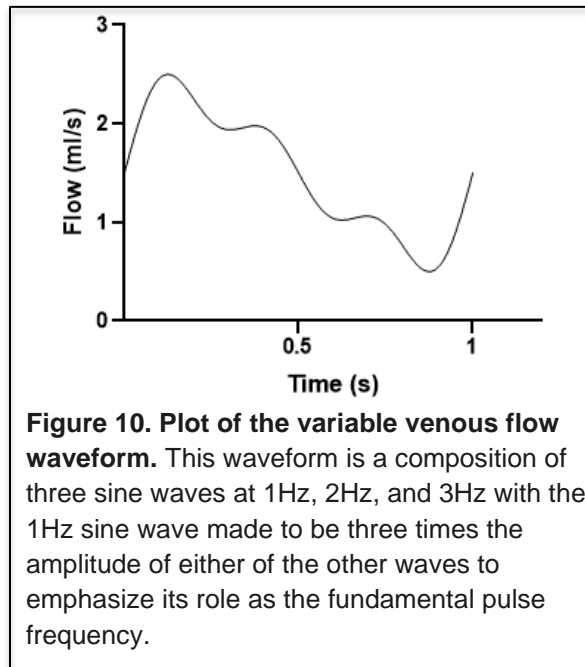
This study used a modified NIVA waveform captured from a porcine saphenous vein cutdown to control pump flow. In early tests of the PVA cryogel phantoms, it was observed that running the porcine NIVA



waveform in the pump resulted in a captured waveform that resembled the derivative of the NIVA waveform itself. This observation led to the creation of the NIVA flow waveform by high pass filtering then integrating the original porcine NIVA waveform. Three consecutive pulse beats were isolated from the resultant waveform for use in the pump. **(Figure 9)** The waveform was normalized to a maximum flow of 5 ml/s as this corresponds to a peak intraluminal pressure of 12 mmHg within the silicone vein embedded within a cryogel.

A synthetic venous flow waveform was also engineered to better study the effect of venous flow rate on the relative powers of f_0 - f_2 . When NIVA transforms a venous waveform into the frequency domain, the venous waveform is being deconstructed into a series of sine waves at relative amplitudes that represent the fundamental pulse frequency and associated harmonics. This process was reversed by summing three sine waves at 1Hz, 2Hz, and 3Hz to mimic f_0 , f_1 , and f_2 of a venous waveform. In this synthetic waveform, the 1Hz sine wave was three times the amplitude of the 2Hz or 3Hz sine wave to highlight

its role as the fundamental pulse frequency. **(Figure 10)** The resultant waveform was then scaled to a peak flow rate of 2.5ml/s to establish a baseline flow waveform called the variable venous flow (VVF) waveform.



2.6) Statistical Tests

GraphPad Prism 9 (GraphPad Software Inc, La Jolla, CA) was used to do the statistical analysis in this study.

2.6.1) Synthetic Vessel Validation

A linear regression was used to determine a slope for the ΔR to pressure relationship for the saphenous vein and each of the silicone vessels.

2.6.2) PVA Cryogel: %HF

The NIVA flow waveform was run through five 6% gel phantoms and four 10% gel phantoms and the resulting waveforms were captured via ADInstruments PowerLabs DAQ sampled at 1 kHz. The amplitudes and

frequencies of the f0:f7 peaks were manually identified in LabChart 7 by fFT using 8k sample windows.

The %HF for each cryogel phantom was computed from the f0:f7 values by **equation (3)**.

In the PVA cryogel experiments, %HF values were first checked for normality using a Shapiro-Wilk test. A two-tailed unpaired t test was used to compare the %HF between the 6% and 10% PVA cryogel phantoms. A ROC curve was used to quantify how well the analysis could differentiate between the softer 6% cryogel and the harder 10% cryogel.

2.6.3) Porcine Myocutaneous Flap: %HF

The NIVA flow waveform was run through fifteen PMF phantoms in the pre-/post- bath states and the resulting waveforms were captured via ADInstruments PowerLabs DAQ sampled at 1kHz. The amplitudes and frequencies of the f0:f7 peaks were manually identified in LabChart 7 by fFT using 8k sample windows.

The %HF for each PMF phantom was computed from the f0:f7 values by **equation (3)**.

The %HF values were checked for normality with both a D'Agostino & Pearson and a Shapiro-Wilks test, then a paired t test was used to directly compare the euvolemic and hypervolemic states. A ROC curve determined if the analysis could differentiate between the euvolemic and hypervolemic states.

2.6.4) Porcine Myocutaneous Flap: Flow

The VVF was ran through five PMF models at three different peak flow rates: 2.5, 5, and 7.5 ml/s by altering the scaling factor in the Compuflow pump control interface (**Figure 11**) and the resulting waveform was captured via PowerLabs DAQ sampled at 1kHz. The amplitudes and frequencies of the f0:f2 peaks were manually identified in LabChart 7 by fFT using 8k sample windows. The NIVA scores and %f0 at each flow rate were computed from the f0:f2 values by **equation (1)** and **equation (2)**.

The NIVA and %f0 values were checked for normality with a Shapiro-Wilks test, then a paired t test was used to directly compare the different flow rates. A ROC curve determined if the analysis could differentiate

between the 5 and 2.5 ml/s flow rates. A linear regression was used to determine the correlation between NIVA score and flow rate.

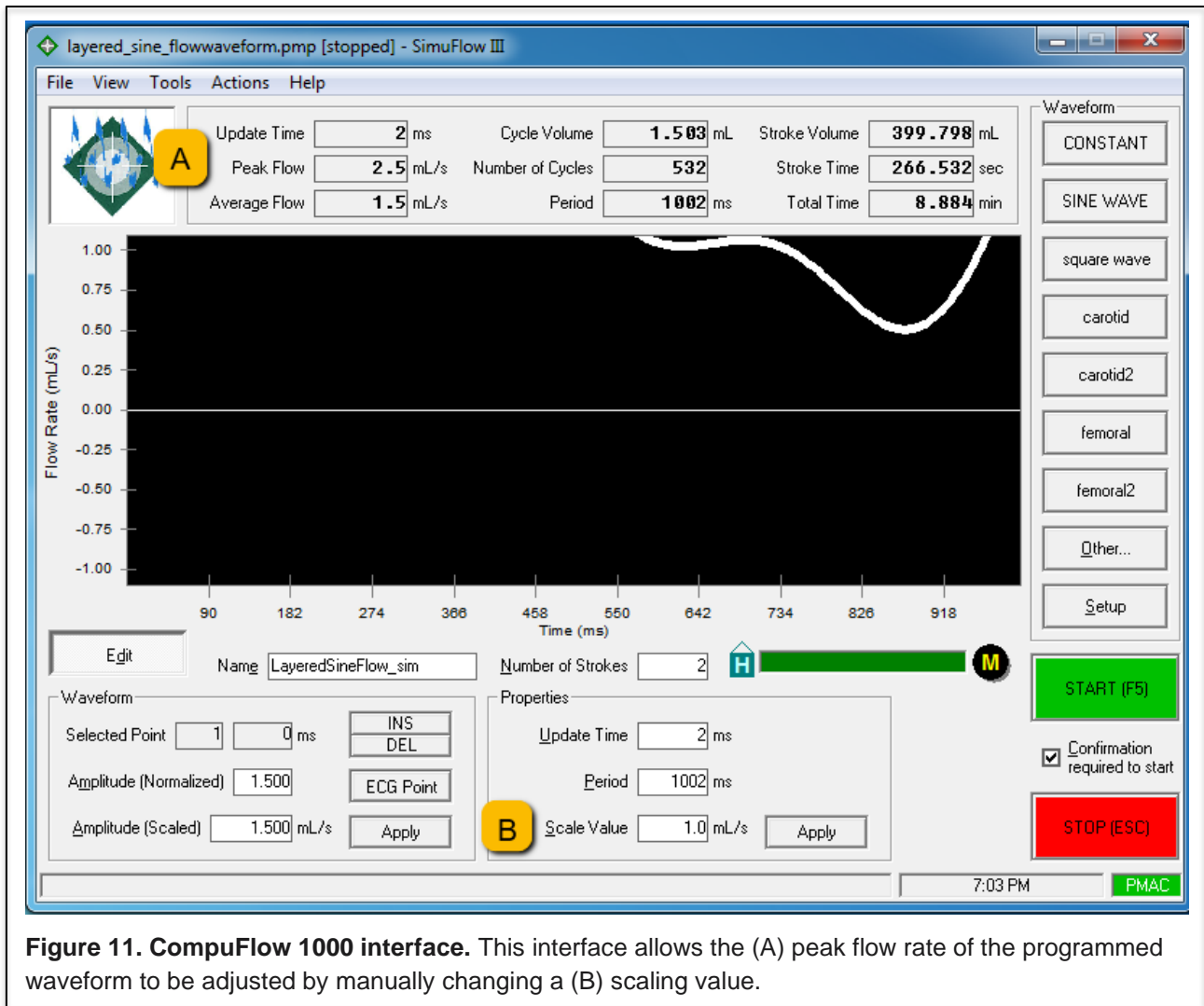
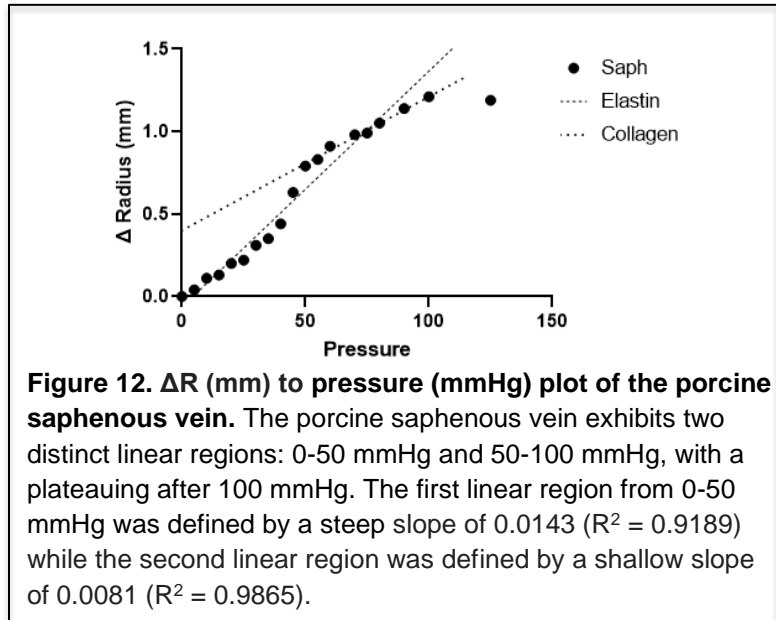


Figure 11. CompuFlow 1000 interface. This interface allows the (A) peak flow rate of the programmed waveform to be adjusted by manually changing a (B) scaling value.

3) Results:

3.1) Synthetic Vessel Validation

The saphenous vein had a Peterson's modulus of 188.64 in the 0 to 25 mmHg range. The EcoFlex 00-30 and 00-50 vessels showed a Peterson's moduli of 101.22 mmHg and 276.67 mmHg in the same pressure range. The OOMOO-25 vessel effectively had a Peterson's modulus of 0 mmHg as it did not meaningfully deform in the 0 to 25 pressure regions.



Plotting the mechanical compliance of

the saphenous vein revealed its absolute rate of deflection. **(Figure 12)** The saphenous vein demonstrated two regions of linear ΔR to pressure relationship, the first of which in the 0 to 50 mmHg range defined by linear regression as:

$$\Delta R = 0.0143P - 0.0641, R^2 = 0.9189 \quad (5)$$

The second linear ΔR to pressure was observed at 50 to 100 mmHg and was defined by:

$$\Delta R = 0.0081P + 0.4, R^2 = 0.9865 \quad (6)$$

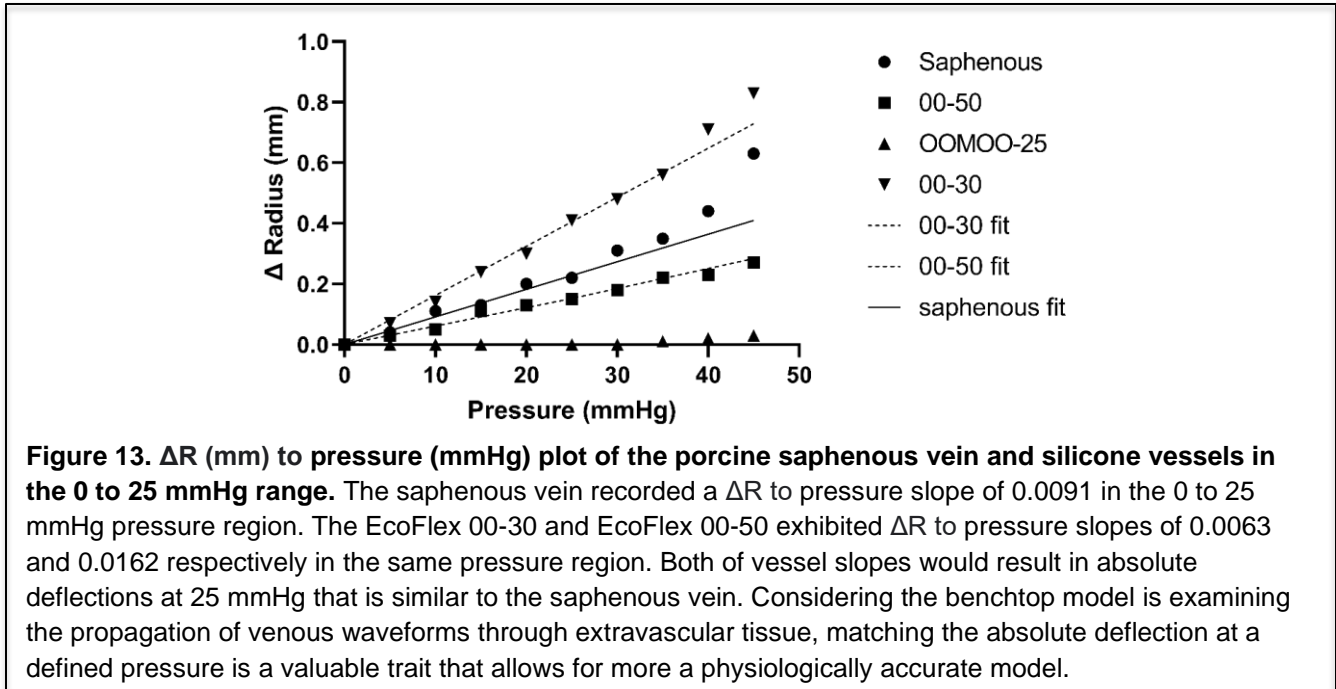
Given that physiologic venous pressures peak before 25 mmHg, the linear fit of the first region **(Equation 3)** can be redefined by restricting it to 0-25 mmHg:

$$\Delta R = 0.0091P + 0.0024, R^2 = 0.9796 \quad (7)$$

A linear fit to the EcoFlex 00-30 and EcoFlex 00-50 vessels in the 0 to 25 mmHg range gave slopes of 0.0063 ($R^2 = 0.9734$) and 0.0162 ($R^2 = 0.9939$) respectively. **(Figure 13)** The OOMOO-25 vessel was disregarded as it did not meaningfully expand in this pressure range. Extrapolating this out to the top end of physiologic

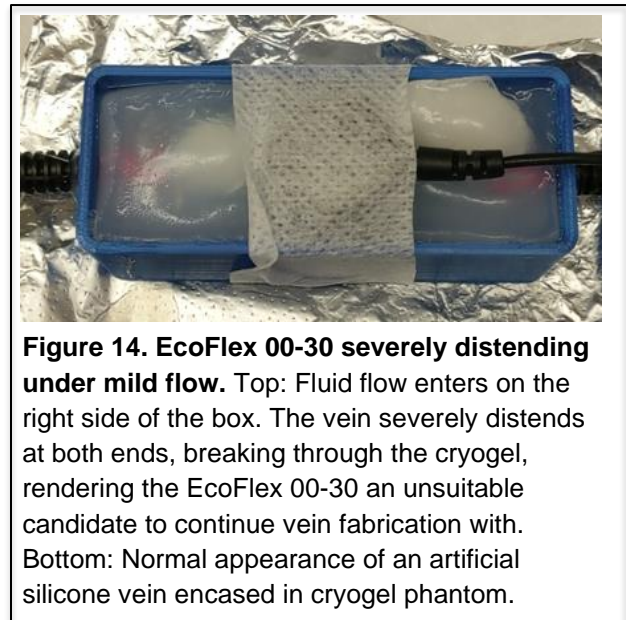
venous pressures at 25mmHg, the expected deflection would be 0.2275mm. The EcoFlex 00-30 and 00-50 vessels would deflect 0.1525mm and 0.405mm respectively under this same analysis.

Both EcoFlex 00-30 and Ecoflex 00-50 were promising candidates to match the performance of the saphenous vein, but EcoFlex 00-30 vessels would routinely not hold up to experimentation. **(Figure 14)**

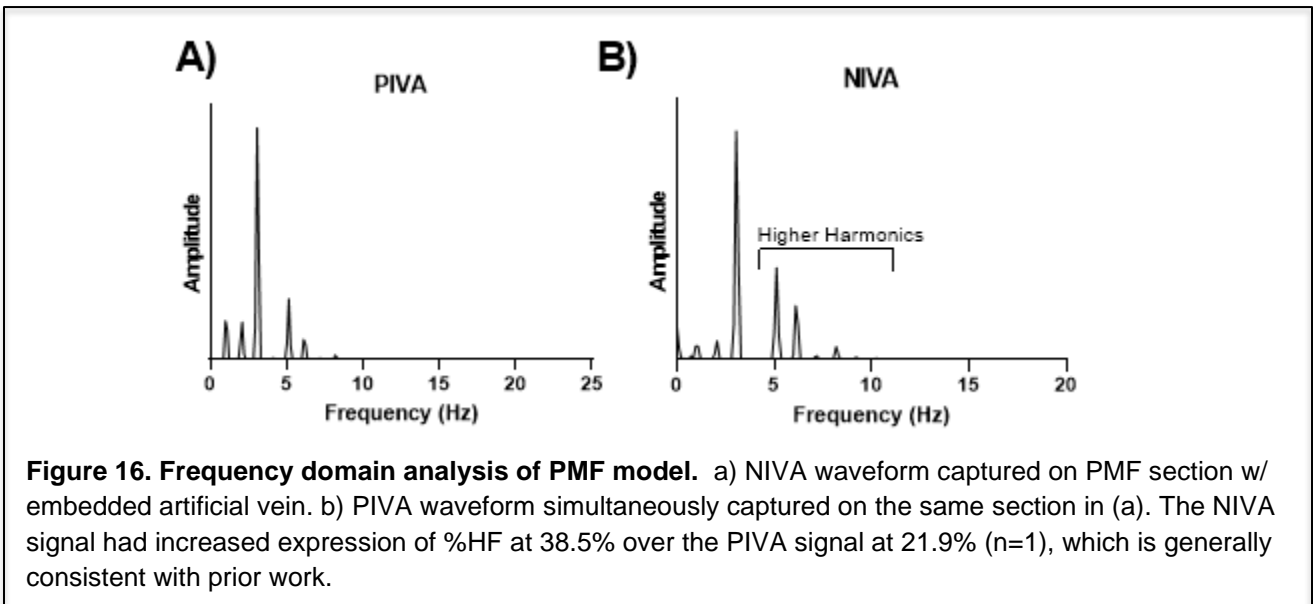
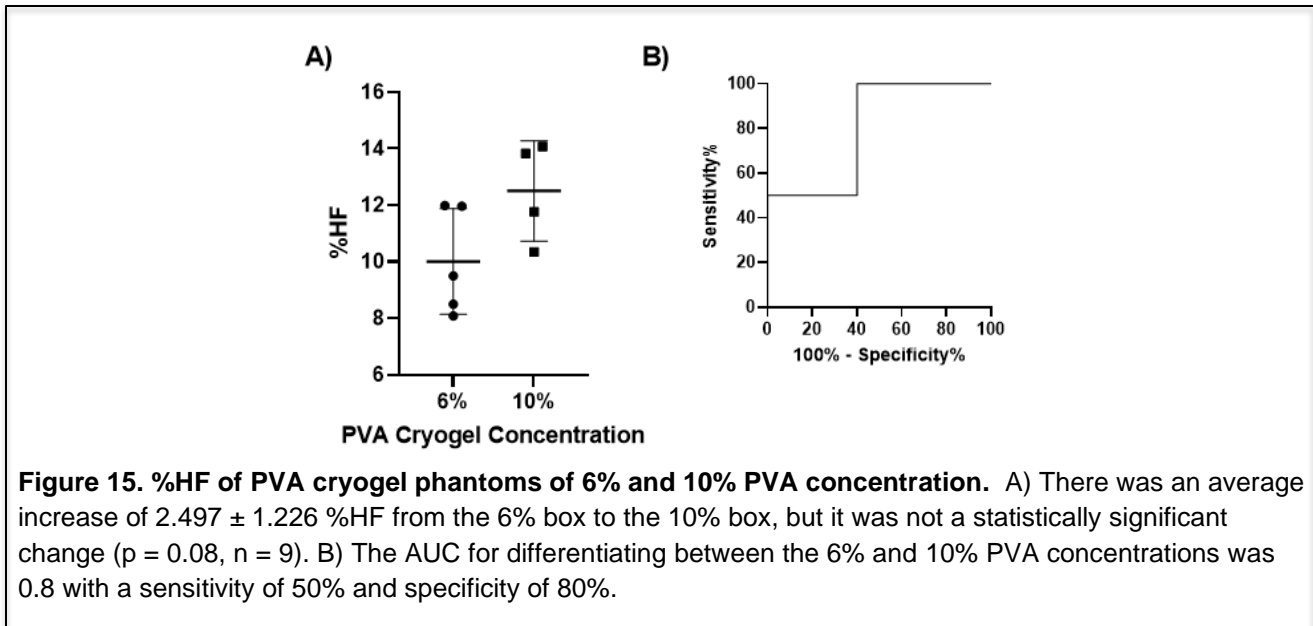


3.2) PVA Cryogel: %HF

Five of each type of PVA cryogel phantom were prepared for experimentation. One of the 10% PVA cryogel phantoms was excluded due to a pump failure during the flow tests. Both the 6% and 10% PVA cryogel phantom groups passed a Shapiro-Wilk test for normality ($W = 0.8414, p = 0.1699; W = 0.8953, p = 0.4081$ respectively).



A two-tailed unpaired t test showed that while there was an average decrease in %HF in the 10% PVA crygel phantoms of $2.497 \pm 1.226\%$, this decrease was not statistically significant ($p = 0.08$). **(Figure 15A)** A ROC curve was used to determine how well the model could show the difference in crygel stiffness. The model predicted an increased stiffness with an AUC of 0.8 at a sensitivity of 50% and specificity of 80%. **(Figure 15B)**

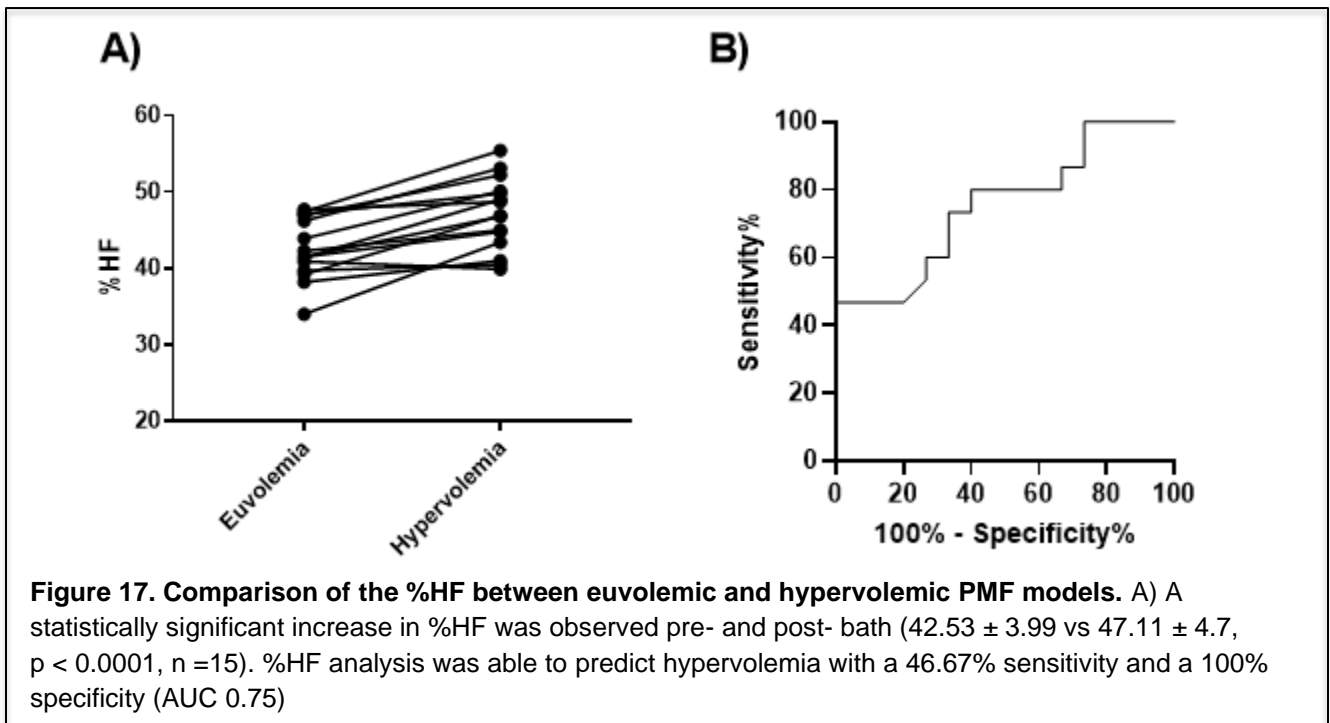


3.3) Porcine Myocutaneous Flap: %HF Modeling

A test run of the modified NIVA flow waveform from the pump revealed that the NIVA signal contained higher harmonic frequencies that were diminished in the PIVA signal. The NIVA signal had a %HF of 38.5% while the PIVA signal only had a %HF of 21.9% (n=1), which is generally consistent with prior work. **(Figure 16)**

A total of 15 PMF flow phantoms were subjected to a 24 hour saline bath to simulate hypervolemia. %HF values pre- and post- bath passed both a D'Agostino & Pearson and Shapiro-Wilk normality tests. A paired two-tailed t-test showed an average increase of 4.6% in %HF in the hypervolemic PMF ($p < 0.0001$). **(Figure 17A)**

The PMF model predicts hypervolemia with a 46.67% sensitivity and a 100% specificity (AUC 0.75). **(Figure 17B)**



3.4) Porcine Myocutaneous Flap Flow Modeling

A total of 5 PMF flow phantoms were used with the VVF waveform to assess the impact of venous flow on the f0-f2 frequencies.

3.4.1) Porcine Myocutaneous Flap Flow Modeling: NIVA

There was a non-zero linear correlation between flow rate and NIVA score. ($R^2 = 0.9574$). **(Figure 18A)** The 2.5 and 5 ml/s groups passed a Shapiro-Wilk normality test ($W = 0.9794$, $p = 0.9316$; $W = 0.927$, $p = 0.7565$ respectively) while the 7.5 ml/s group did not (0.7359 , $p < 0.05$). The 7.5ml/s scores were dropped from further analysis. A paired two tailed t test showed a significant decrease in NIVA score (0.76 ± 0.03 vs 0.55 ± 0.02 , $p < 0.0001$) **(Figure 19A)**

An ROC curve showed that the PMF model perfectly predicts a drop in flow rate from 5ml/s to 2.5ml/s based on NIVA score with a sensitivity and specificity of 100% (AUC 1, $p < 0.01$) at a NIVA score threshold of 0.654. **(Figure 19C)**

3.4.2) Porcine Myocutaneous Flap Flow Modelling: %f0

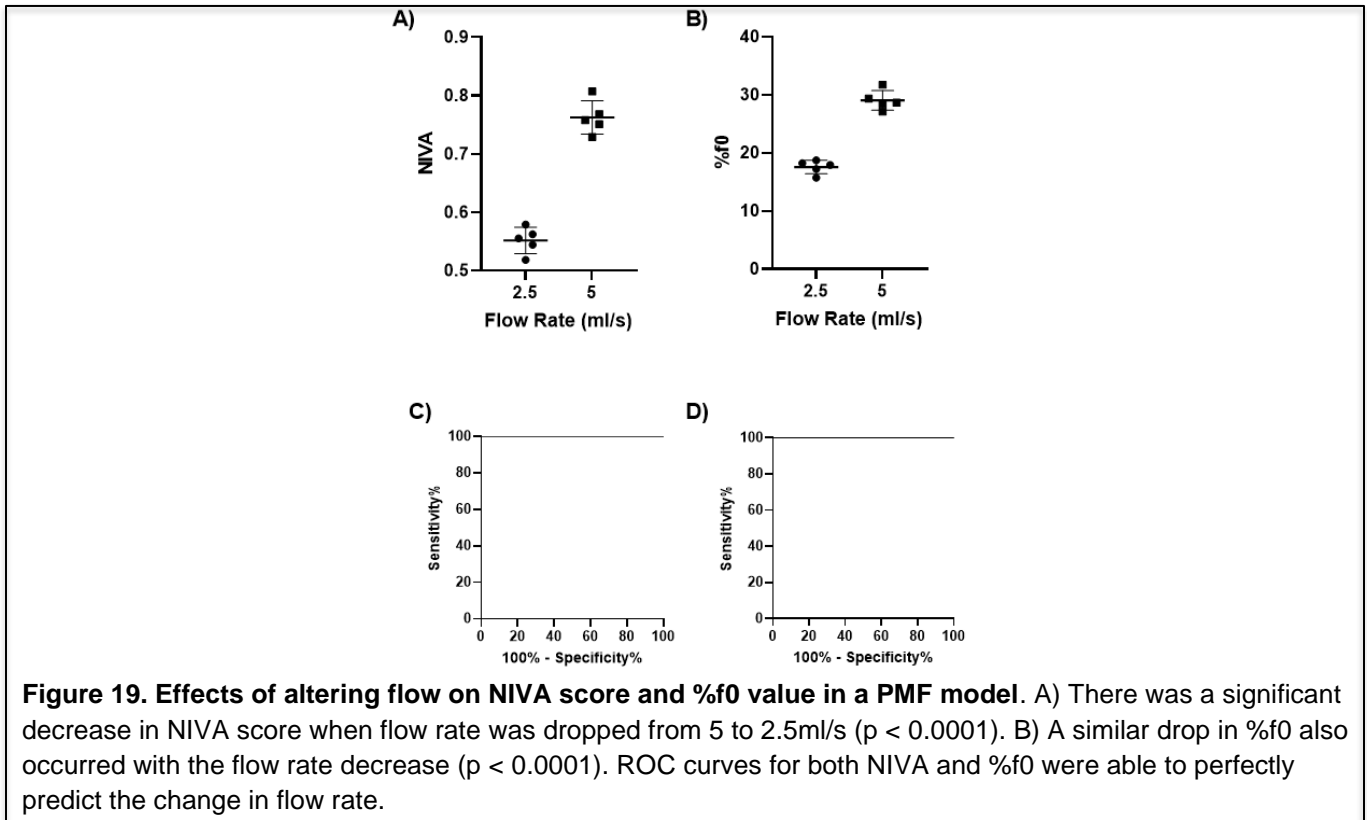
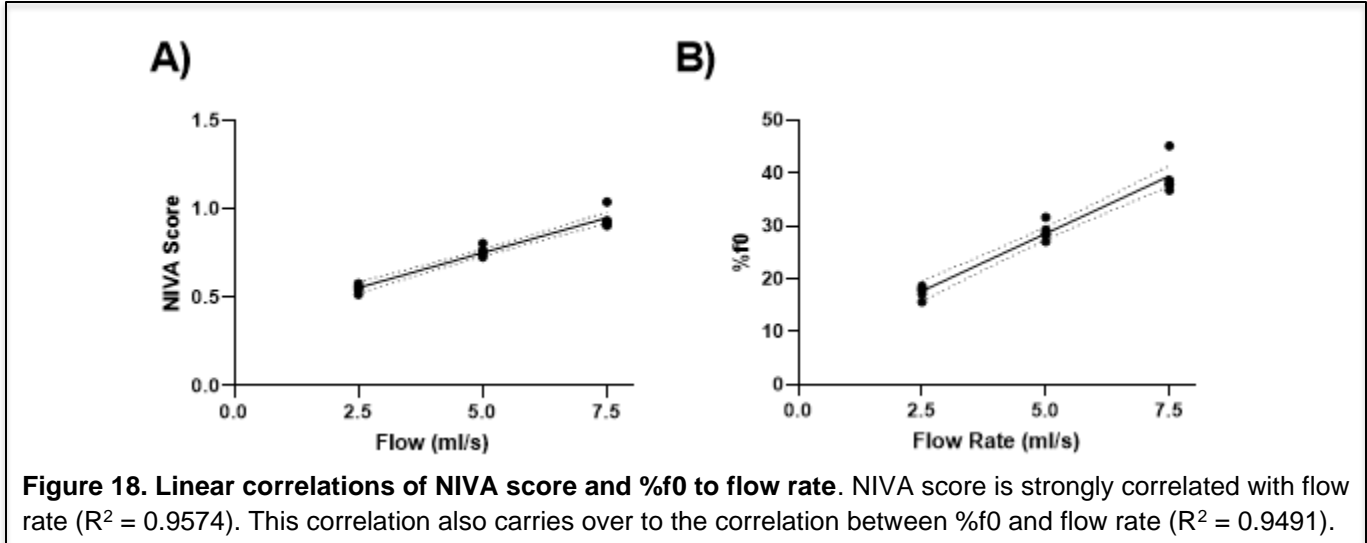
The relative contribution of f0 to the overall NIVA signal was calculated as:

$$f_0/(f_0 + f_1 + f_2)*100 \quad (6)$$

There was a non-zero linear correlation between flow rate and %f0 value. ($R^2 = 0.9491$). **(Figure 18B)**

The 2.5 and 5 ml/s groups passed a Shapiro-Wilk normality test ($W = 0.9232$, $p = 0.5509$; $W = 0.9318$, $p = 0.6085$) but the 7.5 ml/s group did not ($W = 0.7417$, $p = 0.0249$). The 7.5 ml/s values were dropped from further analysis. A paired two-tailed t test showed a significant decrease in %f0 value ($29.02 \pm 1.696\%$ vs $17.54 \pm 1.163\%$, $p < 0.0001$). **(Figure 19B)**

An ROC curve showed that the PMF model perfectly predicts a drop in flow rate from 5ml/s to 2.5ml/s based on %f0 value with a sensitivity and specificity of 100% (AUC 1, $p < 0.01$) at a %f0 value threshold of 22.9%. (Figure 19D)



4) Discussion

4.1) Synthetic Vessel Validation

The compliance testing of the porcine saphenous veins resulted in a curve that can be broken into two distinct regions. **(Figure 12)** At a lower pressure range of 0 to 50mmHg, the saphenous vein exhibited a steep ΔR to pressure slope. At the higher pressure range of 50 to 100 mmHg, the saphenous vein exhibited a shallow ΔR to pressure slope. These findings are consistent with our understanding of how the composition of collagen and elastin in vasculature influence the vascular mechanical compliance. At lower pressures, the more compliant elastin readily uncoils and is uninhibited by collagen, resulting in a larger change in radius per increase in pressure. At higher pressures, the collagen becomes fully uncoiled and begins resisting further distention, resulting in a lesser change in radius per increase in pressure.^{34,38,39} Typically, a nonlinear stress strain curve seen in the saphenous vein is difficult to reproduce artificially. However, if the experimental pressures do not exceed 50 mmHg, the mechanical behavior of the vein is linear in the 0 to 50 mmHg range. Considering the peripheral venous pressure typically tops out at 15 mmHg⁴⁰, this limit is more than acceptable for the synthetic vessels.

The performance of the silicone vessels in the first linear region at 0 to 25 mmHg was quantified in the form of Peterson's moduli, a widely accepted quantifier of vessel mechanical behavior.^{35,36,41} It has been shown that healthy adolescent carotid arteries exhibit Peterson's moduli of 281.27 ± 68.33 mmHg.⁴¹ Considering the arterial pressures are greater than venous pressures, we would expect the vein to have a less stiff modulus. Thus, the EcoFlex 00-30 and 00-50 vessels were accepted as reasonable approximations of saphenous vein based on their Peterson's moduli.

Elastic moduli are but one way to define the relationship between stress and strain. Computation of the ΔR to pressure slopes of the vein and vessels demonstrate that the rate of deflection in the saphenous vein, EcoFlex 00-30, and EcoFlex 00-50 vessels were fairly similar. At the maximum projected pressure of 25

mmHg, we expect only a difference of -0.075 mm in the Ecoflex 00-50 compared to the saphenous vein, while the EcoFlex 00-30 was a slightly worse performer at +0.1775 mm.

Both the EcoFlex 00-30 and 00-50 vessels were promising candidates to mimic the performance of saphenous vein in the 0 to 25 mmHg pressure range. It would have been desirable to test a compound of a Shore 00-40 hardness, but such a material was not readily available. Preliminary flow tests with the EcoFlex 00-30 vessel revealed that it was prone to severe distention under even mild flow rates. **(Figure 14)** Given this issue, it was dropped from consideration as a material for vessel fabrication and the study proceeded with EcoFlex 00-50 as the material of choice.

This validation effort to select EcoFlex 00-50 as a material for synthetic vessel construction is not without some limitations. First, the quantification of the mechanical compliance of the vessels had a low statistical power due to n of 1 of each group. Additionally, the saphenous vein was tested in *ex vivo* conditions. Next, to calculate the venous compliance testing of all the veins it was assumed that the vessel wall was incompressible and thus a static thickness during the tests. This assumption is consistent with those made in prior mechanical tests examining the mechanical compliance of vasculature.^{32,33} Additionally, it was assumed that the saphenous vein was of uniform thickness throughout its length to simplify the compliance calculations.

4.2) PVA Cryogel: %HF

This study used 6% and 10% cryogels to mimic euvoletic and hypervolemic states respectively. It was thought that the extravascular space swollen with excess fluid could be represented by the stiffer 10% cryogel. There was an observed increase in %HF in the stiffer 10% cryogel, however this increase was not statistically significant. The ROC curve also demonstrated a mediocre ability to differentiate between the softer 6% and stiffer 10% cryogels which represents a weakness in identifying peripheral edema and by extension, volume overload. It is thought that this statistical weakness is due to the inconsistency of the crosslinking occurring during the freeze-thaw cycles of the cryogel.

The PVA cryogel was an improvement upon the agar gel in that it allowed for a more granular alteration of its mechanical properties to better mimic physiological conditions. However, the PVA cryogel was not without its own limitations. Originally, it was envisioned that the cryogel could be stratified in different concentration layers to better mimic the layers of myocutaneous tissue. However, the aforementioned inconsistencies in crosslinking at 6% to 10% PVA concentrations lead to concerns that a multi-layer gel would only compound the inconsistencies, so examining single concentration gels were prioritized first. Additionally, the cryogel fails to sufficiently crosslink at any concentrations meaningfully lower than 6%. Seeing how the 6% and 10% PVA cryogel corresponds to normal fatty and glandular breast tissue respectively, the inability to test a composition softer than 6% limits our capability to simulate an abnormal state. Lastly, while silicone is a fairly inert material, repeatedly thermally cycling the artificial vein from -20C to 4C could potentially degrade the vein enough to affect the results. This in sum led to PMF being investigated as an alternative extracellular matrix model to the PVA cryogel.

4.3) Porcine Myocutaneous Flap %HF Modeling

PIVA and NIVA are novel methods of volume assessment that have been proven successful in the clinical setting. A key difference between these two methods is the presence of unique higher pulse harmonics in the NIVA waveform, suggesting that the extracellular matrix is responsible for this difference. The preliminary testing demonstrated that NIVA captured from the PMF model displayed increased contributions of higher pulse frequency as opposed to PIVA captured from the model, corroborating that the extracellular matrix is a key factor in higher pulse harmonic generation.

GDFT is a protocol designed to reduce incidence of complications that arise from fluid imbalance during surgery. However, current monitoring strategies are lacking in being able to correctly guide physicians on fluid resuscitation. An estimated 50% of hemodynamically unstable patients in the ICU or operating room receive unnecessary fluid therapy.⁴² Excessive fluid administration causes a hypervolemic state, which can manifest interstitial edema. Increases in the fluid content in the extravascular tissue that would appear in volume

overloaded patients were modelled by the saline uptake in the PMF during the solution baths. The observed increase in %HF between the euvolemic and hypervolemic states in the model demonstrates that elevated fluid content has an amplifying effect on the relative power of the higher pulse harmonics. The ROC curve reveals that at a threshold of 47.55 %HF, NIVA can predict an euvolemic status with a specificity of 100%. However, at a sensitivity of 46.67% is still a poor diagnosis of hypervolemia in isolation. It is likely this poor sensitivity is a result of the high variability from section to section of PMF in terms of fluid content, composition, and total fluid capacity, much like a real patient would. However, a surgical patient is typically hypovolemic or euvolemic preoperatively depending on urinary output, perspiration loss, and duration of fasting.⁴³ A hypervolemic state is created intraoperatively by overly aggressive fluid administration. Continuous perioperative NIVA monitoring would be able to capture a baseline %HF specific to the individual patient preoperatively to compare intraoperative %HF against to provide clinician feedback on extravascular volume status. Such capability would be of great value clinically, as there currently does not exist any alternative method that can detect intravascular and extravascular fluid excess.⁴²

It should be noted that the modified NIVA flow waveform used in the PVA cryogel and PMF models was derived from a NIVA recording on a porcine saphenous vein cut-down. The piezo-crystal responsible for capturing the NIVA signal does so by generating a voltage when its crystal lattice structure is deformed from a normal state. However, this deformation is more sensitive to changes in lattice deflection rather than the absolute value of the deflection itself. As a result, it cannot be expected that programming a raw NIVA waveform directly back into the Compuflow pump would produce a venous flow. Instead, translation of the captured NIVA waveform into an accurate flow waveform is currently judged largely on the morphology of the resultant waveform. While this NIVA flow waveform is not a point for point reproduction of venous flow, it is believed that it is a close enough representation. Furthermore, it is not believed that work done with an entirely physiologically correct peripheral venous flow waveform would be contradictory to the work completed in this study. The increases in higher pulse harmonics observed in the PMF model stem from the same frequency ranges as increased higher pulse harmonics observed in post-cardiac surgery patients. Given the same

frequency ranges of interest, it is safe to assume that the mechanical resonance generated in the PMF model by the modified NIVA waveform is a good approximation of in-vivo conditions

4.4) Porcine Myocutaneous Flap Flow Modeling

The PMF model was also used to investigate the phenomenon of the fundamental pulse frequency contribution decreasing with hemorrhage in human blood donors.²⁴ There are strong linear correlations between flow rate & NIVA score ($R^2 = 0.9574$) and flow rate & %f0 ($R^2 = 0.9491$) which indicates that NIVA does react to changing venous flow. When acute hemorrhage occurs, the intravascular volume loss reduces the stressed volume that is in part responsible for creating a pressure gradient to drive venous return.³¹ This decreased stressed volume and associated reduction in mean circulatory filling pressure results in a decreased venous flow even in the face of compensatory factors. The ROC curve shows differentiation between the 2.5 and 5ml/s flow rates perfectly by either the %f0 or NIVA metric. That is, if a NIVA score is below 0.654 or a %f0 is lower than 22.9%, the flow rate is certainly decreased and volume loss has occurred. However, there is room to improve the understanding between flow and NIVA/%f0. Adding more flow rates will better clarify the flow-NIVA/%f0 relationship, and increasing the sample size should eliminate the abnormal distribution issue with the 7.5 ml/s NIVA/%f0 measurements.

The blood donor study showed a decrease in NIVA score by ~42% after 500mL of blood donation for an average volume loss of 6.36 mL/kg.²⁴ The PMF models saw a drop in NIVA score by 27.8% when the flow rate was reduced from 5ml/s to 2.5ml/s. A halving of the venous return can be reasonably thought to be much more than a 6.36 mL/kg peak volume loss, so by that logic the decrease in NIVA score should be much greater in the PMF model compared to the blood donors. However, we observe experimentally with the PMF model the opposite of that. The venous system contains 60-70% of the total blood volume and acts as a reservoir.^{26,27,31} When acute hemorrhage occurs, the body will exert neurohumoral control over the venous system to trigger vasoconstriction to compensate for the loss. A NIVA study demonstrated that introduction of a phenylephrine, a

potent vasoconstrictor, in adult pigs led to the NIVA scores dropping by half and the ratio of f_1/f_0 doubling ($p < 0.05$, $n = 8$).⁴⁴ The PMF model currently does not simulate vasoconstriction, so it is likely the lack of this major contributing factor is the leading reason why the PMF model only saw a portion of the decrease in NIVA score compared to the blood donors. Despite the lack of vasoconstriction in the PMF model, there was still a substantial drop in NIVA score and f_0 in the PMF model which is still generally consistent with the human blood donors study. This is a demonstration that decreases in venous return as a result of acute hemorrhage are a substantial factor in changing the venous fundamental pulse frequency in a manner that is readily detected by NIVA.

5) Future Work:

This study focused on comparing the differences between normal and edematous state models. However, the PMF model should allow for study of the dehydrated state and its effects on the PVW. Dehydration occurs at a 2-4% loss of total body weight. A food dehydrator can be used to deplete water contained within the PMF to simulate a dehydrated state. It is hypothesized that a dehydrated state would present a decrease in %HF relative to normal and edematous states. Testing a hypovolemic state will allow for a clearer understanding of the role peripheral venous waveform analysis techniques like NIVA has in improving the GDFT protocol. Furthermore, a dehydrated PMF should be a more accurate extravascular model for the PMF flow experiments, as hypovolemia is associated with hemorrhage.

In regards to improving the venous flow phantom, it also may be possible to utilize an intravascular ultrasound (IVUS) system to capture a flow waveform from a porcine saphenous vein. This would allow for a more physiologically correct sinus waveform to be programmed into the flow pump. However as previously mentioned, it is not thought that this would be contradictory to the work discussed.

6) Conclusion

The development of a benchtop model capable of simulating euvoletic and hypervolemic conditions described in this study provides insight into how changing the fluid content of extravascular tissue impacts noninvasive peripheral venous waveform analysis techniques like NIVA. An increase in fluid content in the PMF model resulted in increases of higher pulse harmonics captured by a piezo-crystal sensor. The confirmation that NIVA can detect interstitial edema in the intraoperative setting on top of its volume assessment capabilities has implications in reducing patient morbidity rates and incidence of complications associated with fluid overload perioperatively. Additionally, it was confirmed in the PMF model that reductions in venous flow have a reductive effect on NIVA scores, which provides insight into the physiological mechanisms that can influence NIVA. Further work in simulating a hypovolemic state may yield valuable information on how to continue developing NIVA as a guide to optimize goal directed fluid therapy.

7) References:

1. Voldby AW, Brandstrup B. Fluid therapy in the perioperative setting – a clinical review. *J Intensive Care*. 2016 Apr 16; 4:27
DOI: 10.1186/s40560-016-0154-3
2. Shin CH, Long DR, McLean D, et al. Effects of Intraoperative Fluid Management on Postoperative Outcomes: A Hospital Registry Study. *Ann Surg*. 2018 Jun;267(6):1084-1092
DOI: 10.1097/SLA.0000000000002220
3. Kang D, Yoo KY. Fluid Management in perioperative and critically ill patients. *Acute Crit Care*. 2019 Nov;34(4):235-245.
DOI: 10.4266/acc.2019.00717
4. Hahn RG, Lyons G. The half-life of infusion fluids. *Eur J Anaesthesiol*. 2016 Jul; 33(7):475-82
DOI: 10.1097/EJA.0000000000000436
5. Reid F, Lobo DN, Williams RN, Rowlands BJ, Allison SP. (Ab)normal saline and physiological Hartmann's solution: a randomized double-blind crossover study. *Clin Sci (Lond)*. 2003 Jan;104(1):17-24.
PMID: 12519083
6. Sjöstrand F, Edsberg L, Hahn RG. Volume Kinetics of glucose solutions given by intravenous infusion. *Br J Anaesth*. 2001 Dec;87(6):834-43
DOI: 10.1093/bja/87.6.834
7. Bellamy MC. Wet, dry, or something else? *Br J Anaesth* 2006. Dec;97(6):755-7
DOI: 10.1093/bja/ael290
8. Benes J, Giglio M, Brienza N, Michard F. The effects of goal-directed fluid therapy based on dynamic parameters on post-surgical outcome: a meta-analysis of randomized controlled trials. *Crit Care*. 2014 Oct 28;18(5):584
DOI: 10.1186/s13054-014-0584-z
9. Bednarczyk JM, Fridfinnson JA, Kumar A, et al. Incorporating Dynamic Assessment of Fluid Responsiveness into Goal-Directed Therapy: A systemic Review and Meta-Analysis. *Crit Care Med*. 2017 Sep; 45(9):1538-1545
DOI: 10.1097/CCM.0000000000002554
10. Makaryus R, Miler TE, Gan TJ. Current concepts of fluid management in enhanced recovery pathways. *Br J Anaesth*. 2018 Feb; 120(2):376-383.
DOI: 10.1016/j.bja.2017.10.011

11. Meng L, PM Heerdt. Perioperative goal-directed haemodynamic therapy based on flow parameters: a concept in evolution. *Br J Anaesth*. 2016 Dec;117(suppl 3):iii3-iii17
DOI: 10.1093/bja/aew363
12. Miller WL, Mullan BP. Understanding the heterogeneity in volume overload and fluid distribution in decompensated heart failure is key to optimal volume management: role for blood volume quantitation. *JACC Heart Fail*. 2014 June;2(3):298-305
DOI: 10.1016/j.jchf.2014.02.007
13. Gelman S, Bigatello L. The physiologic basis for goal-directed hemodynamic and fluid therapy: the pivotal role of the venous circulation. *Can J Anaesth*. 2018 Mar;65(3):294-308
DOI: 10.1007/s12630-017-1045-3
14. Backer DD, Heenen S, Piagnerelli M, Koch M, Vincent JL. Pulse pressure variations to predict fluid responsiveness: influence of tidal volume. *Intensive Care Med*. 2005 Apr;31(4):517-23
DOI: 10.1007/s00134-005-2586-4
15. Wise ES, Hocking KM, Polcz ME, et al. Hemodynamic Parameters in the Assessment of Fluid Status in a Porcine Hemorrhage and Resuscitation Model. *Anesthesiology*. 2021 Apr 1; 134(4):607-16
DOI: 10.1097/ALN.0000000000003724
16. Gödje O, Peyerl M, Seebauer T, Lamm P, Mair H, Reichart B. Central venous pressure, pulmonary capillary wedge pressure and intrathoracic blood volumes as preload indicators in cardiac surgery patients. *Eur J Cardiothorac Surg*. 1998 May;13(5):533-9
DOI: 10.1016/s1010-7940(98)00063-3
17. Johnson SW, Witken A, Rodriguez-Lopez J, Channick R. Room for improvement in pulmonary capillary wedge pressure reporting: a review of hemodynamic tracings at a large academic medical center. *Pum Circ*. 2020 Nov 11;10(4):2045894020929157
DOI: 10.1177/2045894020929157
18. Bitar A, Selej M, Bolad I, Lahm T. Poor agreement between pulmonary capillary wedge pressure and left ventricular end-diastolic pressure in a veteran population. *PLoS One*. 2014 Jan 31;9(1):e87304
DOI: 10.1371/journal.pone.0087304
19. Hocking KM, Alvis BD, Baudenbacher F, et al. Peripheral I.V. Analysis (PIVA) of venous waveforms for volume assessment in patients undergoing haemodialysis. *Br J Anaesth*. 2017 Dec 1; 119(6):1135-1140
DOI: 10.1093/bja/aex271
20. Hocking KM, Sileshi B, Baudenbacher FJ, et al. Peripheral venous waveform analysis for detecting hemorrhage and iatrogenic volume overload in a porcine model. *Shock*. 2016 Oct;46(4):447-52
DOI: 10.1097/SHK.0000000000000615

21. Miles Merrick, Alvis BD, Hocking KM, et al. Peripheral Intravenous Volume Analysis (PIVA) for quantitating volume overload in patients hospitalized with acute decompensated heart failure- a pilot study. *J Card Fail.* 2018 Aug;24(8):525-32
DOI: 10.1016/j.cardfail.2018.05.003
22. Sileshi B, Hocking KM, Boyer RB, et al. Peripheral venous waveform analysis for detecting early hemorrhage: a pilot study. *Intensive Care Med.* 2015 Jun;41(6):1147-8
DOI: 10.1007/s00134-015-3787-0
23. Alvis BD, Polcz M, Huston JH, et al. Observational study of noninvasive venous waveform analysis to assess intracardiac filling pressures during right heart catheterization. *J Card Fail.* 2020 Feb;26(2):136-41
DOI: 10.1016/j.cardfail.2019.09.009
24. Alvis BD, McCallister R, Polcz M, et al. Non-invasive Venous waveform Analysis (NIVA) for monitoring blood loss in human blood donors and validation in a porcine hemorrhage model. *J Clin Anesth.* 2020 May;61:109664
DOI: 10.1016/j.jclinane.2019.109664
25. Sobey JH, Reddy SK, Hocking KM, et al. Non-Invasive Venous waveform Analysis (NIVA) for volume assessment during complex cranial vault reconstruction: A proof-of-concept study in children. *PLoS One.* 2020 Jul 8;15(7):e0235933
DOI: 10.1371/journal.pone.0235933
26. Chang D, Leisy PJ, Sobey JH, et al. Physiology and clinical utility of the peripheral venous waveform. *JRSM Cardiovasc Dis.* 2020 Jan-Dec; 9: 2048004020970038
DOI: 10.1177/2048004020970038
27. Bartelstone HJ. Role of the veins in venous return. *Circ Res.* 1960 Sept;8:1059-1076
DOI: 10.1161/01.res.8.5.1059
28. Mohrman DE, Heller LJ. Hemodynamic interactions, In: Weitz M, Boyle PJ (eds) *Cardiovascular Physiology*. 9th ed. New York: McGraw Hill Professional, Table 1
29. Roth CF, Drees JA. Vascular capacitance and fluid shifts in dogs during prolonged hemorrhagic hypotension. *Circ Res.* 19765 May; 38(5):347-56
DOI: 10.1161/01.res.38.5.347
30. Banet M, Smith EE. Mean circulatory pressure in hemorrhagic shock. *J Appl Physiol.* 1973 Jun;34(6):846-9
DOI: 10.1152/jappl.1973.34.6.846
31. Magder S. Volume and its relationship to cardiac output and venous return. *Crit Care.* 2016; 20(1): 271
DOI: 10.1186/s13054-016-1438-7

32. Brownson KE, Khosravi R, Lee SR, et al. Venous Mechanical Properties After Arteriovenous Fistulae in Mice. *J Surg Res*. 2020 Apr; 248:129-36
DOI: 10.1016/j.jss.2019.12.007
33. Lee YU, Naito Y, Kurobe H, Breuer CK, Humphrey JD. Biaxial mechanical properties of the inferior vena cava in C57BL.6 and CB-17 SCID.bg mice. *J Biomech*. 2013 Sep 3;46(13):2277-82
DOI: 10.1016/j.jbiomech.2013.06.013
34. Vekilov DP, Grande-Allen KJ. Mechanical Properties of Diseased Veins. *Methodist Debaquey Cardiovasc J*. Jul-Sept 2018;14(3):182-87
DOI: 10.14797/mdcj-14-3-182
35. Gosling RG, Budge MM. Terminology for describing the elastic behavior of arteries. *Hypertension* 2003; **41**(6): 1180-2.
DOI: 10.1161/01.HYP.0000072271.36866.2A
36. Peterson LH, Jensen RE, Parnell J. Mechanical properties of arteries in vivo. *Circ Res* 1960; 8(3): 622-639
DOI: 10.1161/01.RES.8.3.622
37. Akki RS, Arunachalam K. Breast tissue phantoms to assist compression study for cancer detection using microwave radiometry. *Annu Int Conf IEEE Eng Med Biol Soc*. 2014:2014:1119-22
DOI: 10.1109/EMBC.2014.6943791
38. Cocciolone AJ, Hawes JZ, Staiculescu MC, Johnson EO, Murshed M, Wagenseil JE. Elastin, arterial mechanics, and cardiovascular disease. *Am J Physiol Heart Circ Physiol* 2018; **315**(2): H189-H205.
DOI: 10.1152/ajpheart.00087.2018
39. Ebrahimi AP. Mechanical properties of normal and diseased cerebrovascular system. *J Vasc Interv Neurol* 2009; **2**(2): 155-62.
PMID: 22518247
40. Choi SJ, Gwak MS, Ko JS, et al. Can peripheral venous pressure be an alternative to central venous pressure during right hepatectomy in living donors? *Liver Transpl*. 2007 Oct; 13(10):1414-21
DOI: 10.1002/lt.21255
41. Baumgartner L, Weberru H, Engl T, Schulz T, Oberhoffer-Fritz R. Exercise Training Duration and intensity Are Associated With Thicker Carotid Intima-Media Thickness but Improved Arterial Elasticity in Active Children and Adolescents. *Front Cardiovasc Med*. 2021; **8**:618294
DOI: 10.3389/fcvm.2021.618294
42. Marik PE, Monnet X, Teboul JL. Hemodynamic parameters to guide fluid therapy. *Ann Intensive Car*. 2011 Mar 21;1(1):1
DOI: 10.1186/2110-5820-1-1

43. Doherty M, Buggy DJ. Intraoperative fluids: how much is too much? *Br J Anaesth.* 2012 Jul; 109(1):69-79

DOI: 10.1093/bja/aes171

44. Polcz M, Hocking KM, Chang D, et al. A brief report on the effects of vasoactive agents on peripheral venous waveforms in a porcine model. *JRSM Cardiovasc Dis.* 2020 Jan-Dec; 9: 2048004020940857

DOI: 10.1177/2048004020940857